Construction and Building Materials 259 (2020) 120394

Contents lists available at ScienceDirect

Construction and Building Materials

journal homepage: www.elsevier.com/locate/conbuildmat

Distribution depth of stone consolidants applied on-site: Analytical modelling with field and lab cross-validation

Matea Ban [a,*,2], Laura Aliotta [b,2], Vito Gigante [b,2], Elisabeth Mascha [c], Antonella Sola [d,1], Andrea Lazzeri [b]

[a] Institute of Geotechnics, Faculty of Civil Engineering, TU Wien, Austria
[b] Department of Civil and Industrial Engineering, University of Pisa, Italy
[c] Institute of Art and Technology, Conservation Science, University of Applied Arts Vienna, Austria
[d] Department of Engineering 'Enzo Ferrari', University of Modena and Reggio Emilia, Italy

HIGHLIGHTS

- Modelling and evaluation of distribution depth of stone consolidants.
- Colloidal suspensions exhibit an exponential decline to varying degrees.
- Drilling resistance shows over-consolidation which agrees with the applied model.
- Deposition of consolidants inside the stone determines a treatment's performance.
- Mechanical tests confirm the treatments efficiency (i.e. mechanical strength gain).

ARTICLE INFO

Article history:
Received 1 February 2020
Received in revised form 22 July 2020
Accepted 24 July 2020
Available online 1 September 2020

Keywords:
Analytical modelling
Stone consolidation
Distribution of consolidants
Scanning electron microscopy
Drilling resistance

ABSTRACT

An analytical model was applied in order to understand the distribution depth of cured stone consolidants. The model is grounded on a case study of Vienna's St. Stephen's Cathedral and was verified against drilled cores examined by SEM and image analysis, on-site drilling resistance measurements and laboratory-based mechanical tests. The results reveal that the variation of the concentration gradient with penetration depth resembles an exponential decline. The deposition of the cured consolidant is governed by capillary forces upon drying within water-based nano-zirconia dispersions and water/alcohol-based colloidal silica. This effect is less pronounced within reactive consolidants, which undergo polycondensation reactions, as with alkoxysilanes.

1. Introduction

Preservation of architectural surfaces is a common practice, and for such purposes, new materials are continuously being developed and modified. One of the most demanding tasks in built heritage preservation is the restoration of the physical characteristics and mechanical properties of a building's surface that has naturally aged. These surfaces usually exhibit a degradation pattern, more severe at the exposed surface and less so towards the inner structure of the building's wall material. To restore such complex patterns, various stone consolidants are frequently applied. These consolidants differ in chemical, physical and mechanical properties, and the choice and study of their interaction with a substrate is often grounded on a case-by-case basis, considering certain stones or architectural surfaces. Occasionally, a combination of consolidants is used to remedy problems regarding damages of varying sizes [1]. Moreover, efforts have been made to modify particle size and shape to overcome decay patterns of different magnitudes and to treat substrates of higher porosities [2]. Some consolidant modifications include the functionalisation of surfaces to retard further decay caused by e.g. biological colonization [3] or water penetration [4]. Some common consolidants include metal oxides and colloidal silica in various solvents as well as alkoxysilanes that form a silica gel that strengthens the substrate. Furthermore, synthetic organic polymers, calcium hydroxide, ammonium

* Corresponding author.
E-mail addresses: matea.ban@tuwien.ac.at (M. Ban), laura.aliotta@dici.unipi.it (L. Aliotta), vito.gigante@dici.unipi.it (V. Gigante), elisabeth.mascha@uni-ak.ac.at (E. Mascha), antonella.sola@unimore.it (A. Sola), andrea.lazzeri@unipi.it (A. Lazzeri).
[1] Present address: Commonwealth Scientific and Industrial Research Organisation, Manufacturing Business Unit, Metal Industries Program, Clayton, VIC, Australia; antonella.sola@csiro.au.
[2] These authors contributed equally to the work.

https://doi.org/10.1016/j.conbuildmat.2020.120394
0950-0618/

oxalate or hydroxyapatite are just few additional consolidants frequently used in architectural preservation.

A consolidation treatment is undertaken by applying the liquid consolidant on the monument stone so that it penetrates into the stone matrix. Consequently, the consolidant reacts by evaporation of the solvent or chemical reactions to form a coherent material in the stone structure, thereby strengthening the stone monument. The latter process is known as curing; within this process, the treatment's performance depends on several variables. The mode of application is known to influence the outcome [5,6], as is the solid content of the consolidant after curing [7]. Furthermore, the role of the solvent has been proven to be crucial for the penetration depth and thus for treatment performance [8]. The macro- and micro-climatic conditions on-site are important for chemical reactions and evaporation processes. All these variables make this field of scientific study active and vivid, particularly as many of these processes can be assessed only by analytical and numerical modelling. Regarding the latter, the transport and deposition of stone consolidants on-site are one of the processes that can be studied only with numerical modelling, as there is no method available allowing examination of the penetration and distribution depth of consolidants into a building wall. Furthermore, it is important to know where the consolidating material is deposited inside the stone structure after the curing process because the consolidant needs to strengthen the identified decay patterns without any harmful effect. Harmful effects of a consolidation treatment could include over-consolidation of the surface, pore clogging or a deeper penetration and consolidation of sound bulk material, causing differential strength profiles. Study of consolidant deposition is crucial in the field of architectural preservation, but consolidant distribution alone does not give information about treatment efficiency. The efficiency of a treatment must be evaluated through physical tests.

The laboratory affords various possibilities for studying the efficiency of a consolidant: tests of splitting tensile strength, bending strength, compressive strength or pull-off adhesive strength. On-site, only a few methods are capable of providing evidence for mechanical strength gain. The methods used on-site to study mechanical strength include drilling resistance and sound speed propagation. Every method of study is accompanied by certain limitations, and experience has shown that only with a combination of on-site and laboratory-based methods may reliable results be achieved [9]. As an example, scanning electron microscopy (SEM) allows direct observation of pore clogging phenomena. Additionally, SEM can give insights into the consolidant's properties of adhesion to the pore walls of the substrate and the distribution or bridging capacities of the consolidating material. However, SEM cannot provide evidence regarding the actual strength of the consolidated material, which can be achieved by e.g. drilling resistance measurements.

Neutron imaging shows a great potential in stone conservation analysis [10]. With neutron imaging, the inner structure of a material can be analysed, as can the liquid that flows through it. This technique was used to investigate the deposition of consolidants inside natural stones [11–13], but such large-scale imaging facilities are not easily accessible. The complementary method, which is available on laboratory scale, is X-ray microtomography, which has shown promising results in a study that scanned the stone before and after treatment [14]. However, when the substrate under study and the consolidating material share the same chemical composition (i.e. carbonates consolidated with nano-calcite) and little consolidant is applied, no technique makes it easy to obtain precise measurements of consolidant distribution after curing. The latter issue is more easily assessed through SEM analysis, as the higher spatial resolution allows the differentiation of textural changes between the stone and consolidant. Microscopy in combination with image analysis is particularly helpful in assessing coverage of coatings for protection of architectural surfaces [15].

Studies dealing with the flow or deposition of consolidants inside a stone structure using analytical or numerical modelling are not common in the field of built cultural heritage. Fractal modelling is the most widely used method to describe the movement of liquid in a pore network system of porous materials [16]. It is rather the related disciplines of geoscience and environmental science, as well as nuclear waste disposal, that have focused on modelling phenomena regarding reactive transport, sorption and diffusion [17,18]. Predictive modelling of phenomena in the field of the built cultural heritage, although essential, is lacking in terms of published research.

The present work provides an analytical approach that allows, through simple calculations, the analysis of consolidant depth distribution. Thanks to the final equation's basis in theoretical analysis, this method can be easily applied by specialists on-site. The present study provides an improved evaluation tool for treatment performance. Three consolidants, namely, i) water-based nano-zirconia dispersion, ii) water–alcohol-based colloidal silica and iii) nano-titania-modified alkoxysilane, were applied on-site, on a porous calcarenite. Drilled cores have been extracted from the monumental site and investigated, in the laboratory, by SEM and image analysis to obtain information on the distribution depth of the consolidant's solid content after curing. Analytical modelling proved capable of describing the degree of exponential decline of the concentration gradient with penetration depth and could also fit the experimental data in a satisfactory way, allowing explanation of differences in deposition pattern among the studied consolidants. The focus of the work was finding possible explanations for differences in deposition profiles of the examined consolidants and, where possible, to provide predictive indicators of their performance. Example drilling resistance measurements on-site and lab-based mechanical tests (i.e. sound speed propagation and splitting tensile strength) helped support the modelling-based evaluation of treatment effectiveness.

2. Experimental section

2.1. Building stone

The stone studied in this work is a calcareous arenite, sourced from lower Austria's Burgenland and known under the name of the quarry, *St. Margarethen*. It is a white to yellowish porous calcareous arenite consisting of calcite found in the form of fragments of coralline red algae, bryozoans, echinoids and foraminifers as well as traces of quartz (<1 wt%), as seen in Fig. 1**a**. The porosity of this sedimentary lithotype amounts to ~ 20 vol%, with aggregates reaching sizes of a few millimetres, cemented with fine crystalline calcite (see Fig. 1**b**). This lithotype is still quarried and used for restoration purposes, especially in Vienna and lower Austria. It exhibits typical decay patterns of granular disintegration, microcracking and black crusts. Because it is prone to chemical weathering and freeze–thaw cycling [19], conservation treatment is unavoidable. However, high porosity and variable morphology of damaged *St. Margarethen* makes the choice regarding a proper conservation treatment difficult. Please refer to Supporting Information for more details on petrographic and petrophysical features.

2.2. Consolidation treatment On-Site and in laboratory

The on-site testing area is located at the south façade of St. Stephen's Cathedral in the city centre of Vienna, Austria. The buttress used for this pilot study originates from the beginning of the 20th

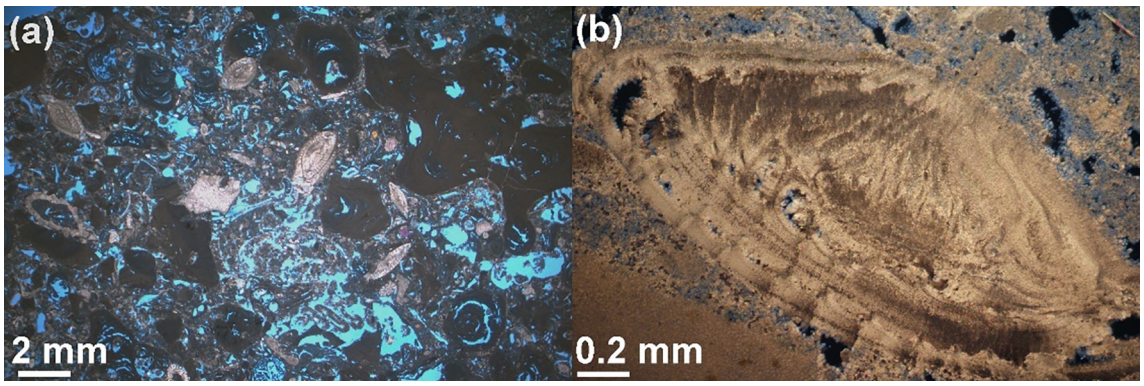

Fig. 1. a) Microstructure of freshly quarried *St. Margarethen* as observed in thin section under parallel-polarised light using a Nikon optical microscope. **b)** Detail of a foraminifera fragment surrounded with the binding medium, a fine crystalline calcite cement observed in cross-polarised mode. Blue and black space represents the resin used for embedment of the stone specimens. (For interpretation of the references to colour in this figure legend, the reader is referred to the web version of this article.)

century, and it exhibits extensive granular disintegration and the formation of black crusts (see Fig. 2). Granular disintegration is a generic term describing lost cohesion between the grains of a substrate, whereas the formation of black crusts is a form of mineral replacement reaction to the detriment of calcite that can be traced to the activity of sulphate agents and environmental pollutants [20]. For detailed information about the predominant decay patterns found on-site and a condition assessment, see Supporting Information.

The preparation of the surface involved sensitive mechanical and chemical cleaning, with micro chisels and poultice of ammonium bicarbonate, respectively. However, an accurate removal of the gypsum in depth was not possible due to the severely damaged surface. A careful steam cleaning was carried out before consolidants were applied. The application of the three consolidants, listed in Table 1, was done by the run-off method using pipettes until refusal of the consolidant was visible. This procedure was repeated the next day, having in total a treatment application of two cycles. The curing involved a loose 1 week coverage with foil to protect the treated surface from sun and rain exposure and to avoid a too fast evaporation.

The consolidants were developed during a recently finished Horizon 2020 project known as 'Nano-Cathedral', short for 'Nanomaterials for conservation of European architectural heritage developed by research on characteristic lithotypes' (Grant Agreement No. 646178). The exact routes of synthesis for these consolidants are therefore protected by non-disclosure agreements, as industrial partners were involved in product development. However, the project ensured a high technology readiness level (TRL) of these newly engineered materials. They have been validated in laboratory and relevant environment, including a development of technical and safety data for their use. For specialists on-site, industrial products are more relevant than consolidants developed by academic researchers as the latter often fail to be implemented on-site, also due to liability reasons. Most consolidants used in construction work are industry developed products.

The effectiveness of each consolidant, that is, its capability to increase mechanical strength after treatment, was assessed in a laboratory-based study using sound speed propagation and splitting tensile strength. For that work, freshly quarried *St. Margarethen* samples were artificially aged by heat treatment to induce micro-cracks in the substrate. The ageing procedure is described elsewhere [21] and involved preliminary studies concerning residence time, cycles and heating rates to achieve microstructural defects that reduce the soundness of the stone without macroscopic failure (i.e. large cracks traversing the specimen). Thermal stresses are commonly employed for ageing purposes prior to stone consolidation studies [22]. In the present study, the stone samples were placed in an electrical furnace (model Heraeus K114 from Thermo Scientific) with a heating rate of 40 °C min^{-1} until the target temperature of 600 °C was reached and maintained for 1 h. A rapid cooling of approx. 15 min to room temperature followed. When the specimens reached room temperature, the procedure was repeated. A total of three heating cycles were completed. For more details on the effect of artificial ageing please refer to Supporting Information.

Consolidation in the laboratory was performed by capillary absorption for 1 h on the bottom side of each specimen (i.e. the lower side was left dipped in a vat of consolidant for 1 h while the lateral sides were sealed with a parafilm sealing tape) that was equilibrated under laboratory conditions (22 ± 3 °C, ~50% RH) beforehand. Thorough penetration of the specimens by the consolidant was ensured by visual inspection. In fact, as often happens with water, the movement of the wetting front of the consolidant progressively changed the colour of the stone (i.e., darkening) and this allowed to follow the penetration of the specimens with the naked eye. A total of two consolidant application cycles were completed, with 24 h between the two applications. Afterwards, the specimens were loosely covered with a polyethylene foil for 1 week, simulating on-site aftercare conditions. After treatment, the samples were weighed for 1 month once per day in order to determine when equilibrium was reached. Testing of the specimens was done 2 to 3 months after consolidation, to ensure that sufficient curing time for complete alkoxysilane polymerisation had passed. The latter point was particularly important as a polycondensation reaction might be ongoing for an indefinite period, as reported by other authors [23,24].

It is important to note that a direct comparison of specimens treated on-site and in the laboratory cannot be made, but rather the latter should serve as supporting information in evaluating on-site tests. Treatment application on-site and in laboratory is not comparable and might lead to varying treatment performances. Specifically, the applicability of the lab-based treatment method (i.e., capillary rise from one side) cannot be mimicked on-site and variable factors (e.g. gravity, pressure, precision, contact area, etc.) might influence a treatments outcome. Moreover, on-site conditions, including micro- and macro-climate, decay pattern variation and application amount, cannot be properly mimicked in the laboratory and require further efforts in research analysis. Nevertheless, laboratory-based methods are good indicators for a treatment's effectiveness [9] and a necessary step in evaluating newly engineered consolidants. Details regarding the amount of consolidants applied on-site and in laboratory can be seen in Supporting Information.

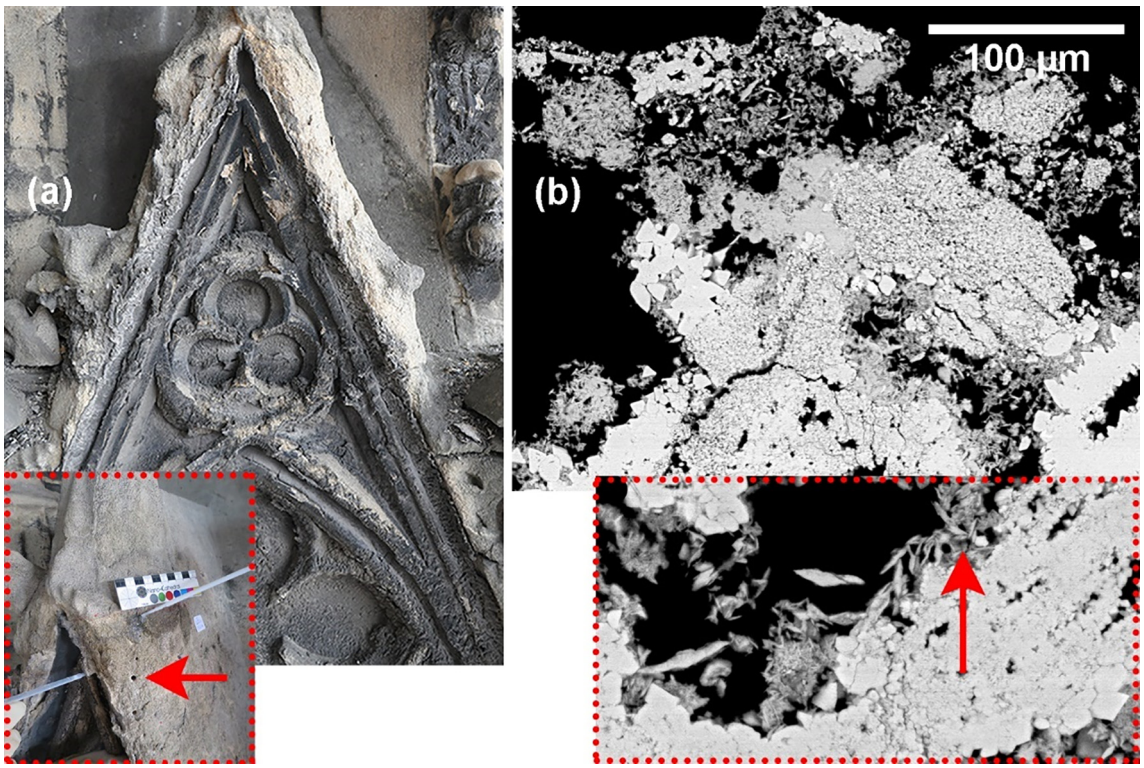

Fig. 2. a) Architectural element on the south façade of St. Stephen's Cathedral used as the testing area. Inset shows the surface during application of a consolidant and the drilling resistance holes made for the purpose of testing the condition prior to treatment (red arrow). **b)** Typical decay pattern, observed in back-scattered mode on polished thin sections, exhibiting damage more pronounced at the surface. Inset shows the presence of gypsum in the microstructure, visible in the form of needles (red arrow). (For interpretation of the references to colour in this figure legend, the reader is referred to the web version of this article.)

Table 1
Characteristics of the studied stone consolidants.

Project labelling	Commercial name (producer, country)	Materials chemistry	Dimension of Nanoparticles (nm)	Concentration in wt% (***)
NC-25C	HFES 70 (ChemSpec, IT)	Nano TiO_2 (1%) mod. TEOS(*) in isopropanol	10–20 TiO_2 (**)	47 ± 0.5
NC-12C	ZG12 (Colorobbia, IT)	SiO_2 in water/ethanol	~70	23 ± 0.5
NC-29C	ZR110 (Tecnan, ES)	ZrO_2 in water	~119	11 ± 0.5

(*) Tetraethyl orthosilicate, also known under the general term alkoxysilane and abbreviated as TEOS, with the chemical formula $Si(OC_2H_5)_4$. (**) Contains approx. 80% anatase and 20% rutile. (***) The solid content after curing was calculated on laboratory treated specimens by dividing the residue weight of the consolidant after curing, assessed approx. 2 months after application, by the applied weight of consolidant and multiplying by 100 to obtain percent; using 10 specimens with a dimension of 5 × 5 × 5 cm. Note that the mass of NC-25C might deviate with time due to ongoing polycondensation reactions. .

2.3. Characterisation

Characterisation of the naturally weathered and consolidated building stone included SEM examination on extracted drilled cores and subsequent image analysis. Moreover, to cross-validate the findings, drilling resistance was performed on-site in the vicinity of the holes that originated from extracted drilled cores used for image analysis. Additionally, sound speed propagation and splitting tensile strength were tested on laboratory specimens for the purpose of studying mechanical strength gain after consolidation.

The polished cross-sections were observed by SEM (Philips XL 30 ESEM), at 20 kV under low vacuum, using back-scattered electrons and employing energy-dispersive X-ray analysis. Detailed phenomena such as adhesion were studied at high magnification (normally 200x to 1500x, mostly 400 x), whereas SEM micrographs, taken at low magnification of 100x, were assembled using Photoshop® to observe the full depth of a sample and analyse the distribution depth of a given consolidant. Analysed depth was limited to approximately 10 to 15 mm. SEM studies were also done on laboratory-treated specimens to validate on-site observations.

The image analysis process was carried out using the software ImageJ [25] (v 1.51r, National Institutes of Health, Bethesda, MD, USA). In that analysis, each image was divided into vertical columns, and each column-like micrograph was again subdivided into horizontal bands 1 mm in height. The consolidant, within the structure of the stone, was mapped using false colours. For each band, the volume fraction occupied by the consolidant was calculated as the fraction of false-coloured pixels in the image. In this way, the concentration of solid content after curing was determined as a function of depth within the stone. An average concentration profile and corresponding standard deviation were calculated over two subdivisions of each micrograph prior to modelling. The assumption made in the SEM analysis was that all the consolidant (i.e. 100% of its solid content) applied at the specimen's surface was contained within the analysed specimens and, in particular, within the depth observed in the image.

Drilling resistance measurements were performed on-site with a DRMS cordless device developed by SINT Technology s.r.L. (Italy). Drilling resistance measures the resistance in Newton to a penetration force. It is calculated as a function of the speed of rotation, the

penetration speed, the drill bit diameter and the material tested. The rotation speed of 600 rpm and the penetration speed of 10 mm/min were kept constant. The penetration depth amounted to 15 mm, comparable with the image depth analysed by SEM. A custom-made 5 mm polycrystalline diamond bit was used for each treatment evaluation, which obviated the need for a correction for drill bit wear. The drilling resistance test was performed before treatment application and 1 year after application on-site.

Determination of the dynamic modulus of elasticity, by measuring the fundamental resonance frequency, was performed by longitudinal study on each of three prismatic specimens (1 × 1 × 4 cm) in their pristine, artificially aged (i.e. heat treated) and subsequently consolidated states according to EN 14146 [26]. The tested size ensured that the consolidants penetrated the entire body of each specimen. A Conosonic C2-GS ultrasonic pulse generator, a pair of UP-DW transducers and a notebook preinstalled with Light House Touch software, all developed by Geotron-Elektronik (Pirna, Germany), were used. The device used was equipped with a built-in algorithm that calculated the dynamic modulus of elasticity, Ed_L, in GPa, obtained from the measured longitudinal fundamental resonance frequency F_L as

$$Ed_L = 4 \times 10^{-6} \times l^2 \times F_L^2 \times \rho \times T \quad (1)$$

where l represents the length and ρ the density of the stone. The correction factor T can be assumed to equal 1, as the width of the specimens is four times its length, so Eq. (1) is simplified by the correction factor.

The test method for splitting tensile strength, investigated according to ASTM D3967 [27], was implemented with an Austro Test Hrdina GmbH MA-CO89 four-column hydraulic servo control loading device. The testing setup consisted of a flat bearing block at the bottom and a curved bearing block on the top of the stone specimen. Cardboard bearing strips of 0.6 mm thickness were used to reduce the contact stresses. An average was calculated from six specimens of diameter of 6 cm and thickness of 3 cm. The splitting tensile strength σ_t in MPa was determined as

$$\sigma_t = \frac{2P}{\pi LD} \quad (2)$$

where P represents the maximum load applied in Newtons as indicated by the testing machine, and L and D correspond respectively to the thickness and diameter of the specimen in mm.

An overview of the analysis carried out on *St. Margarethen* treated on-site and in laboratory as well as the methods used to investigate the treatments performance can be viewed in Table 2.

Table 2
Analysis carried out on *St. Margarethen* treated on-site and in laboratory.

Type of test (Standard)	On-site	Laboratory	Note
SEM-EDX (Not Stand.)	Yes (1)	Yes (2)	(1) One drilled core, 2 cm in diameter, per test area (i.e., consolidant) extracted.(2) One specimen per consolidant.
PLM (Not Stand.)	Yes	No	Condition assessment and damage analysis in combination with SEM-EDX. Three specimens were extracted on-site for damage analysis.
Drilling resistance (Not Stand.)	Yes	No	Distance of bore holes before and after treatment application approx. 2 cm. Low-destructive test.
Drying behaviour (EN 16322)	No	Yes	Average of three samples (5 × 5 × 5 cm) per consolidant with daily monitoring for four weeks.
Dynamic elastic modulus (EN 14146)	No	Yes	Average of three samples (1 × 1 × 4 cm). Direct comparison of sound, artificially aged and consolidated conditions. Non-destructive test.
Splitting tensile strength (ASTM D 39967)	No	Yes	Average of 10 samples per condition (i.e., sound, artificially aged and consolidated). Destructive test.

(1) For modelling purposes, doing false colour mapping using Photoshop® and ImageJ. (2) Analysis of details regarding bridging capacity, cracking and adhesion to substrate.

2.4. Analytical model to describe the distribution depth of the consolidant after curing

An analytical model was obtained to evaluate the quantity, as a function of depth, of consolidant present in the building stone, following an on-site treatment with three consolidants. The first approximation to model this phenomenon is to view the system (i.e. stone and consolidant) as a filtering system in which the stone acts as a filter against the consolidant that passes through it. In the literature, this approach is usually found in studies concerning oil recovery. The probabilistic sieve model describing microfiltration [28–30], used to analyse pore blocking processes, allows the determination of physicochemical parameters of nonstationary filtration phenomena of aqueous suspension.

In the present case study, the driving forces that carry the consolidant through the stone's fabric are capillary forces. In order to evaluate the concentration of consolidant c as a function of depth ×, a mass balance is applied in the following form:

$$V\frac{dc}{dx} = D\frac{d^2c}{dx^2} \quad (3)$$

where D is the diffusivity and V the filtration speed of the studied system. As equilibrium conditions are reached (i.e. the curing of the consolidant completes), time dependence becomes negligible. Therefore, the boundary conditions to solve Eq. (3) are

$$B.C.\begin{cases} c(x=0) = c_0 \\ c(x=L) = c_L \end{cases} \quad (4)$$

where C_0 is the solid content concentration found on the stone's surface at the end of the curing process and C_L is the solid content concentration at the maximum depth reached by the treatment within the analysed sample volume. As the system is described to be a filtration system, where the treated stone is the filter, the expression of velocity follows Darcy's law [31,32]. Therefore, the effective filtering speed V is connected to Darcy's speed V_D according to the following relation:

$$V = \varepsilon \cdot V_D = -\frac{k}{\mu}\frac{\Delta P}{L} \quad (5)$$

In Eq. (5), the negative sign of the term on the right-hand side provides for positive values of the velocity in the direction of the motion. The suspension viscosity is given by μ, whereas k is the permeability and $\Delta P\ L^{-1}$ the pressure drop over a given distance. ε represents the average porosity of the stone, evaluated using image analysis as described above. The permeability indicates the capability of a viscous fluid to penetrate a porous system and can be evaluated through experimental tests or, for well-known systems, found in the literature [33,34]. Otherwise, as a first approximation, the Blake–Kozeny relation (eq. (6)) can be used to calculate the stones permeability k in terms of the average pore diameter D_p and stone porosity ε as follows:

$$k = \frac{{D_p}^2 \cdot \varepsilon^3}{150 \cdot (1-\varepsilon)^2} \quad (6)$$

As capillarity is the driving force of this system, it obeys the Young–Laplace equation:

$$\frac{\Delta P}{L} = \frac{2\sigma cos\theta}{{R_p}^2} \tag{7}$$

where σ is the surface tension, θ the wettability (contact angle) and R_p the pore radii of the system. Inserting Eqs. (6) and (7) into Eq. (5), the final expression of filtering velocity is obtained. Solving Eq. (3), the degree of solid content concentration as a function of sample depth can be described as an analytical solution as follows:

$$\left[-\frac{2D_p\sigma cos\theta}{75\mu DL}\cdot\frac{\varepsilon^3}{(1-\varepsilon)^2}\right]\frac{dc}{dx} = \frac{d^2c}{dx^2}. \tag{8}$$

In Eq. (8), it is possible to define the following parameters:

$$A = \frac{\varepsilon^3}{(1-\varepsilon)^2} \tag{9}$$

$$B = \frac{2D_p\sigma cos\theta}{75\mu DL}, \tag{10}$$

where A is a function of the stone's effective porosity, evaluated by image analysis as the weighted average along the depth of the stone, and B is an empirical parameter obtained through mathematical iterations (using the Generalized Reduced Gradient (GRG) method until the convergence was obtained), encompassing the wettability, average porous dimensions, permeability and diffusivity of the macroscopic system. Substituting the starting boundary conditions (Eq. (4)) into Eq. (8), we obtain the following solution:

$$c(x) = \frac{e^{-ABx}(C_0\cdot(e^{ABL}-e^{ABx}) + C_L\cdot e^{ABL}(e^{ABx}-1)}{e^{ABL}-1} \tag{11}$$

which can be rewritten in the following form:

$$c(x) = \frac{(C_L-C_0)\cdot e^{-ABx} - (C_L-C_0) + C_0\cdot(e^{-ABL}-1)}{e^{-ABL}-1} \tag{12}$$

The solution given through Eq. 11 or 12 makes it evident that the distribution of the solid content after curing follows an exponential growth or decline. To estimate the adequacy with which the obtained equations describe the distribution depth of the consolidants, they have been verified in relation to the values obtained from image analysis. The mathematical rearrangement from Eq. (12) to Eq. (11) can be viewed in Appendix I.

3. Results and discussion

3.1. Image analysis and analytical solution for the distribution depth of consolidants

SEM analysis provided the basis for the development of the analytical model as well as the evaluation procedure. The image-analysed distribution depth for all three consolidants can be seen in Fig. 3.

Additional information obtained through SEM analysis regards the adhesion of the consolidants onto the grain surfaces and the bridging capacity between grains. The latter is correlated with cracking of the consolidating matrix. The SEM results are summarised in Table 3, with examples shown in Fig. 4**a–d**. SEM analysis shows that the nanoparticle-based consolidants exhibit better adhesion and bridging capacities than alkoxysilane. The poor adhesion and bridging of NC-25C can be attributed to drying stresses and thus its susceptibility to cracking.

The micrographs analysed and reported in Fig. 3 indicate that the solution of the differential equation based on the stone used as a filter represents a good methodology to model the complex system. In fact, Eq. (12) fits very well with the experimental data for all the studied consolidants, as can be seen in Fig. 5. The experimentally assessed and thus modelled curves exhibit exponential decline to different extents.

The curves in Fig. 5 show that NC-12C and NC-29C deposit preferentially on the stone surface compared to NC-25C. NC-12C exhibits a more pronounced accumulation of solid content in the subsurface area, through the first 3 mm of sample depth. This slight difference from NC-29C might be related to the more volatile solvent, namely, a water/ethanol mixture. The fast solvent evaporation of the consolidated stone was further confirmed through gravimetric analysis for the determination of solid content reported in Table 1 and displayed in Fig. 6. It is evident that NC-12C and NC-29C exhibit an equilibrium mass after ~ 5 days of weighing, whereas treatment NC-25C requires approximately 4 weeks to establish equilibrium under laboratory conditions. Therefore, an accumulation of solid content after curing on the surface and in the subsurface zone can be related to a back-migration of particles, carried with the solvent during evaporation (see Fig. 6**b**). Specifically, the first drying phase is governed by capillary forces; only during later stages, the drying behaviour changes and can be attributed to diffusion velocities (i.e. vapor diffusion). Franzen and Mirwald already demonstrated such a process in natural stone using water [35]. The present study confirms that such behaviour is also present for colloidal water and water/ethanol systems.

Treatments NC-12C and NC-29C show comparable distribution depth behaviour after curing, which is distinguishable from that of treatment NC-25C. NC-25C shows the most promising depth distribution, possibly explained through its chemistry. Namely, the higher relative humidity and temperature on-site favour an immediate gelation of the consolidant. Moreover, the pore walls of an on-site object might contain more water, thereby catalysing polymerisation more effectively. An initiated gelation would hamper a back-migration of the consolidant and could have a positive effect on the distribution of the consolidant inside the stone.

The analytical model can be evaluated using two approaches. The first possibility is to describe the results through the two terms obtained from Eqs. (9) and (10). The first term A, in Eq. (9), corresponds to the image-analysed porosity after consolidation (i.e. concentration of solid content that remained inside the stone). In contrast, the term B, found in Eq. (10), is more difficult to analyse, as it describes a variety of physical parameters, which, if assessed experimentally one by one, could provide advanced insights (and not average, mathematically derived values) that possibly fit with more precision to the experimental data. Both terms are evaluated in Table 4.

It is evident that the stone structure exhibits a range of porosities, given by term A, even though the examined drilled cores belonged to the same architectural element. This explanation is intuitive, as the material under study is a highly heterogeneous stone, consisting of many fragments of various shapes and dimensions. The term B describes phenomena such as permeability and diffusivity, which are linked to structural changes. Moreover, wettability of crystalline material also depends on microtextural variations and chemical composition, evident in various samples of the stone. However, neither term can be explained solely through the substrate; the interaction of the consolidant with the substrate plays a role as well. Studies concerning the latter are lacking in published research. As an example, it is not known how different wettabilities influence a reaction between consolidant and substrate or how a colloidal suspension diffuses with respect to varying roughnesses or distributions of pore radii. Such processes would involve the study of capillary or interfacial forces, surface complexations and electrostatic interactions, to name few phenomena that would need to be considered when assessing the interaction of substrate and consolidant. Nonetheless, a second

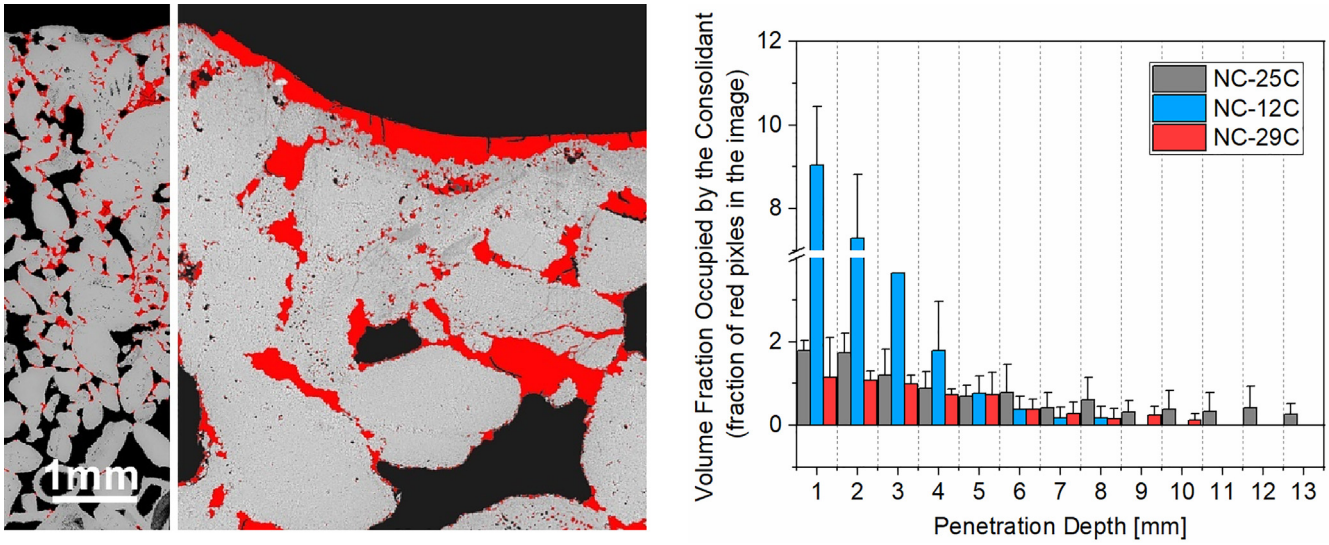

Fig. 3. Left: Example of distribution depths of a consolidant, assessed by image analysis and false-colour mapping. **Right:** A graph displaying the volume fraction occupied by the consolidant in the stone structure as a function of sample depth.

Table 3
Qualitative SEM analysis of polished cross-sections of the treated stone.

Treatment	Distribution depth (*)	Adhesion between stone and consolidant	Bridging between grains
NC-25C (HFES70)	~15 mm	+	average of ~ 50 μm
NC-12C (ZG12)	~10 mm	+++	up to 100 μm
NC-29C (ZR110)	~10 mm	+++	up to 100 μm

(*) The distribution depth is limited through the sample size analysed. Coding for the evaluation of adhesion: (**+++**) good and (**+**) poor.

possibility for evaluating the analytical model and giving predictive indicators of treatment performance lies in modifying the well-known exponential function $f(x) = e^x$, with the following constants added to the equation:

$$c(x) = C_1 + C_2 \cdot e^{(-c_3 \cdot x)} \quad (13)$$

The constants are obtained by a basic nonlinear exponential curve fitting using the software OriginPro®. Herein, constant C_1 describes the offset from the Y axis, constant C_2 describes the offset from the X axis and constant C_3 relates to the vertical exaggeration of the exponential curve. An evaluation based on Eq. (13) is often used in cases in which exponential phenomena play a role, as is the case with degradation patterns [36]. All constants found in Eq. (13) are also reported in Table 4 for each of the three consolidants.

Empirical meanings of these constants can be extrapolated from the real-world results. A higher C_1 value, in the present case the value that is closer to zero, indicates deeper distribution, corresponding to the concentration of consolidant at the maximum analysed depth in the specimen. This value does not correspond solely to the distribution depth of solid content of consolidant but also to the ratio of consolidant and to the stone porosity at a given depth. The term C_2 relates to the term C_1 as it describes the difference between the concentration present on the surface and that present at the maximum analysed depth in the sample. The C_2 value gives insights into the homogeneity of the distributed consolidant from the surface to the analysed depth. The lower the C_2 value, the more homogeneous the distribution is along the depth transect. As regards the exponential coefficient of the distribution depth curve given by C_3, lower values indicate that the distribution is more homogeneous along the depth transect. The higher the C_2 and C_3 values, the more solid content is placed in the near-surface zone. However, these interpretations are based on a mathematical treatment of the constants, in which the concentration of solid content is not considered. That is, if the same distribution of fitted points on the curve is present but with higher values, the constants yield the same values, underestimating the importance of the solid content concentration. Still, C_2 and C_3 are valuable indices for mechanical differentiation stresses that can come about if more consolidant is present at the very surface followed by an abrupt concentration change at shallow depth. Such distributions might cause an over-consolidation of the near-surface zone. It is important to note that consolidant distribution is itself an incomplete criterion, since more solid content might be needed in the vicinity of the surface, where a more pronounced decay is usually found. To deepen the above described mathematical evaluation regarding a treatment performance, the consolidants used must be further evaluated with mechanical tests.

Finally, the used approach to mathematically describe the distribution depth could be extrapolated for the entire monument. However, it should be noted that an extended diagnostic is necessary. As different micro and macro climatic conditions are found on-site, with varying exposures, different decay patterns will be present. This might have an influence on a treatment's performance and thus the distribution depth of applied consolidants. Nevertheless, the used approach can help identify various parameters that possibly influence a penetration depth (e.g. state of the substrate, application cycle, application method, curing conditions, type of consolidant, etc.). This methodology allows for an advanced description and a possible preparation of a model that takes more physical and chemical phenomena into account.

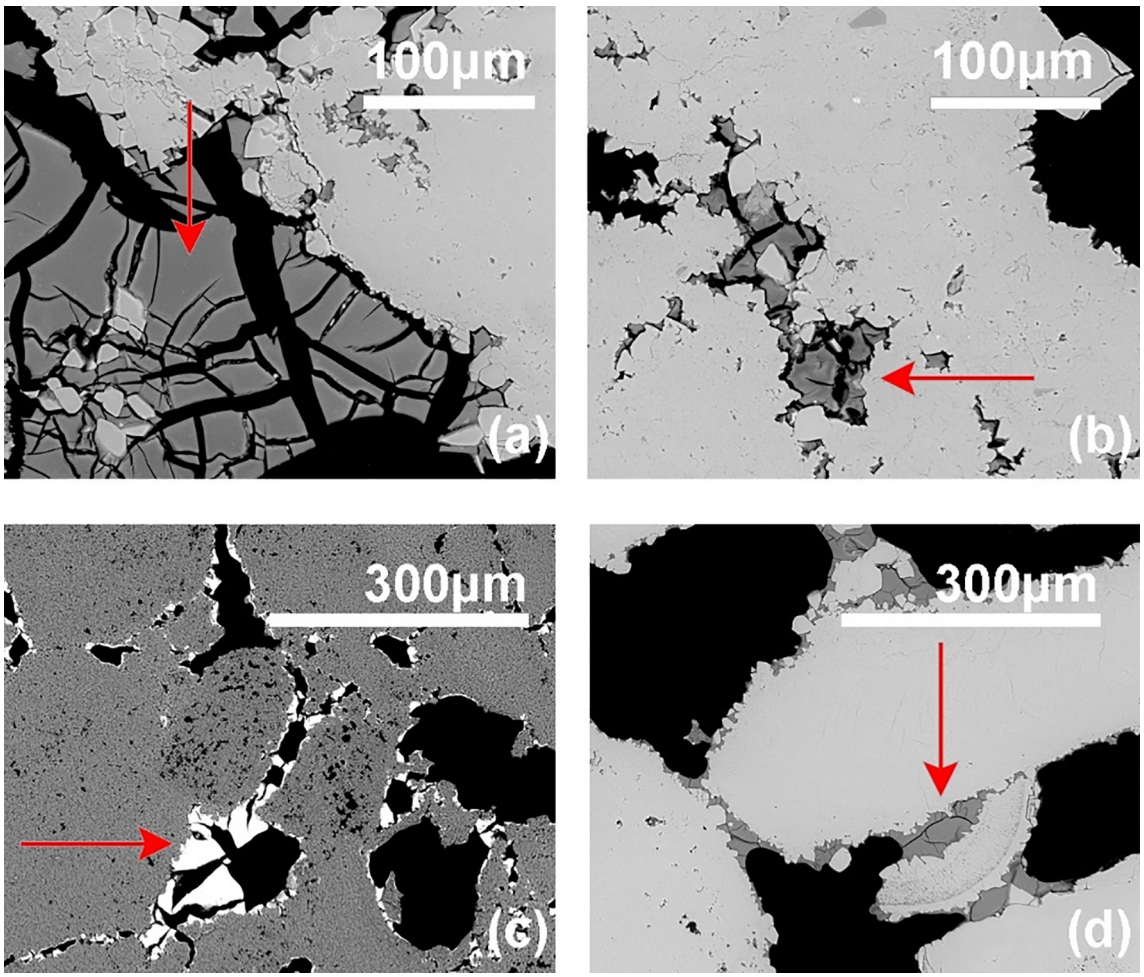

Fig. 4. Example micrographs of laboratory-treated stone showing consolidant properties. **a)** Cracking present in the silica gel matrix of consolidant NC-25C. **b)** Partially loose silica gel plates of NC-25C in the pore space. **c)** Good adhesion between *St. Margarethen* and nano-zirconia (NC-29C). **d)** Good adhesion between *St. Margarethen* and nano-silica (NC-12C).

3.2. Cross-validation with mechanical tests

Mechanical tests performed on-site after application of consolidants included drilling resistance measurements in the vicinity of the SEM analysed samples (approx. distance of 2–3 cm), whereas mechanical tests performed in the laboratory included sound speed propagation tests as well as splitting tensile strength tests on sound, artificially aged and treated samples. The results from drilling resistance measurements performed before and after the treatment can be seen in Fig. 7. The outcome clearly mirrors the results obtained through SEM image analysis. In particular, an exponential decline is also visible through drilling resistance measurements, for treatments NC-12C and NC-29C. Both of those consolidating materials exhibited an over-consolidation in the first two millimetres, where the surface became higher in strength than at higher penetration depths. However, consolidation treatment was necessary, as conveyed by all the drilling resistance values prior to treatment. That is, the very low values of drilling resistance prior to consolidation reveal that the weathered stone was initially of low mechanical strength and that the surface was disintegrated. After treatment, an increase in drilling resistance was observed for all three consolidants, implying some restoration of the strength of the material. It is important to note that the starting stone conditions are different for different samples even under a single consolidant's treatments, as observed in Fig. 7**c** within treatment NC-29C. In that case, a surface higher in drilling resistance was already present before the consolidant was applied. Such situations are most probably caused by the presence of gypsum inside the stone structure, as observed by SEM (see Fig. 2**b**).

Such over-consolidation phenomena might pose a danger by setting up strong differences in mechanical and physical properties in the material and abrupt transitions (i.e. higher strength at the very surface, decreasing drastically as in the cases of NC-12C and NC-29C). Consequently, over-consolidation can result in spalling or pore clogging. However, more research concerning such phenomena is needed in order to assess the effectiveness and compatibility of a given consolidant that exhibits over-consolidation. Micromechanical and nanomechanical studies of various consolidants [37] should be performed in order to assess the cohesion of the consolidant. In addition, macroscopic mechanical tests should be performed with different stiffnesses present in the stone [38] in order to assess the cohesion of the consolidated stone. Furthermore, a possible way to overcome the accumulation of the consolidant near the surface, if caused by a back-migration, could be pretreatment of the surface (e.g. prewetting with alcohol) or a more controlled aftercare until curing completes. Likewise, cyclic treatments or different application techniques might help control the outcome of a treatment's depth distribution. A promising method might be the overlapping application of multiple consolidants to combine their advantages.

Further laboratory mechanical analysis included the determination of the dynamic modulus of elasticity and the splitting tensile

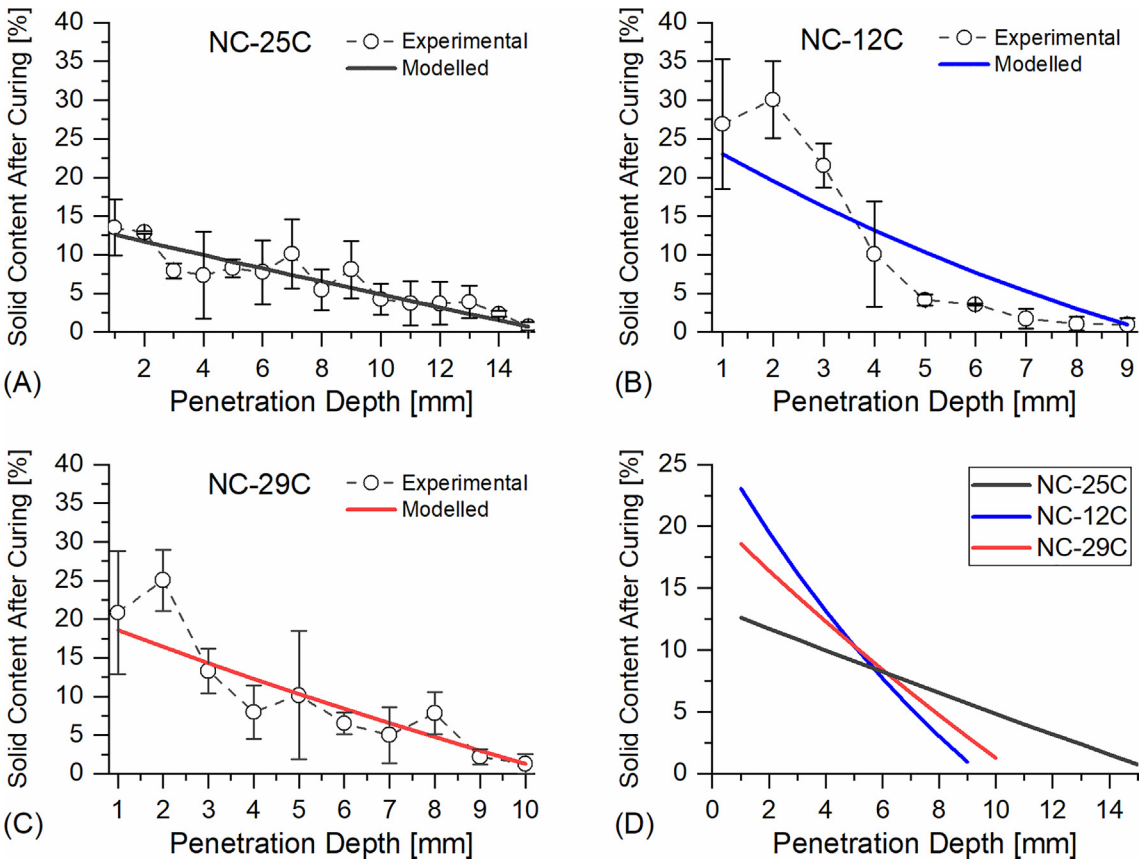

Fig. 5. Comparison of experimental (symbols) and modelled curves (lines) obtained from image analysis of the drilled cores and the analytical model, respectively, for **a)** NC-25C (titania-modified alkoxysilane), **b)** NC-12C (nano-silica) and **c)** NC-29C (nano-zirconia). **d)** Overlap of all three treatments as obtained through the analytical model, to emphasise the differences in their depth distributions. The Y axis displays the percentage connected to solid content after curing as a function of the stone's effective porosity.

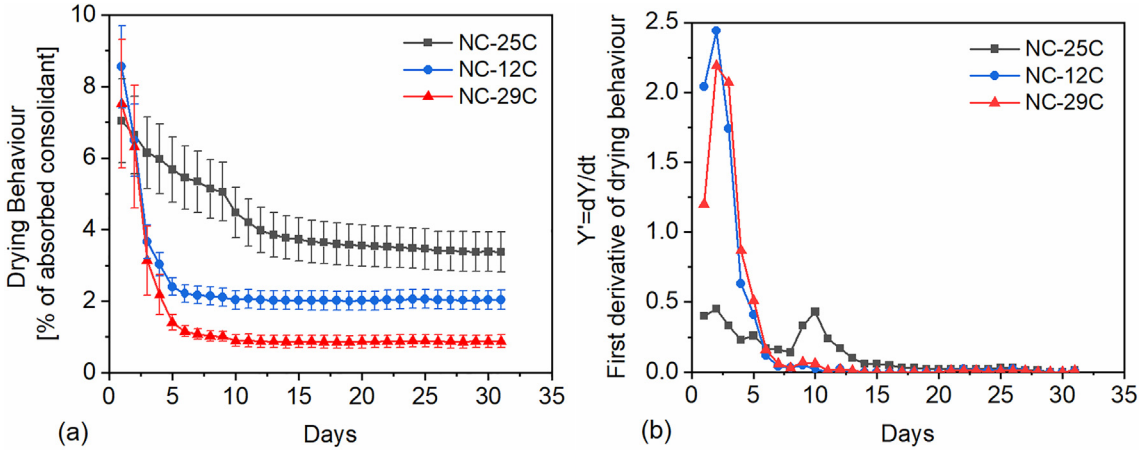

Fig. 6. a) Gravimetric monitoring of the mass loss recorded after consolidation, for a total of 30 days. The height at equilibrium corresponds to the amount of solid content residue in the stone structure, as determined for three specimens with dimensions 5 × 5 × 5 cm under laboratory conditions (~50% RH, ~22 °C). **b)** First derivative of the mass loss to indicate the importance of capillary forces during the first days of drying for treatments NC-12C and NC-29C.

Table 4
Constants A and B calculated from image analysis and iterated through the analytical model, respectively. And, constants C_1 to C_3 used to assess the treatments performance, as evaluated through the modified exponential function in Eq. (13).

Treatment	A	B	C_1	C_2	C_3
NC-25C (HFES70)	0.09	0.08	−28.042	41.555	0.024
NC-12C (ZG12)	0.09	0.85	−30.936	57.849	0.064
NC-29C (ZR110)	0.04	0.69	−53.270	74.096	0.031

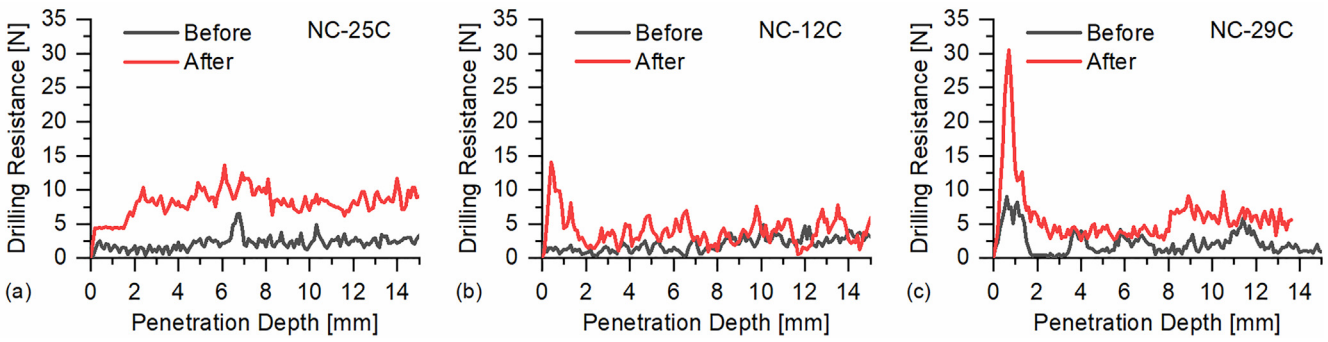

Fig. 7. Drilling resistance measurements performed on-site on *St. Margarethen* before and after treatment with **a)** NC-25C, **b)** NC-12C and **c)** NC-29C.

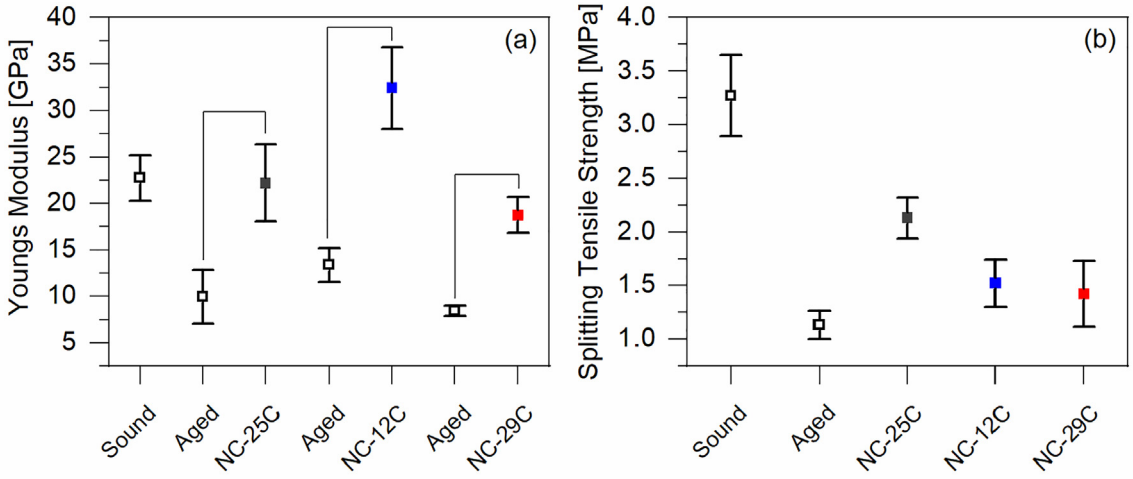

Fig. 8. a) Young's modulus and **b)** splitting tensile strength tested on sound (fresh), artificially aged (heat treated) as well as artificially aged and subsequently consolidated specimens treated in the laboratory. Please note that for the determination of the Young's modulus (Fig. 8a), the same specimens were tested in different conditions (non-destructive testing method), while the determination of splitting tensile strength (Fig. 8b), was carried out on different sets of samples (destructive testing method).

strength. These data supported the findings obtained on-site through drilling resistance measurements, as can be seen in Fig. 8.

The Young's modulus increased after the application of each of the three treatments and equalled or exceeded the values of the sound or fresh stone. Judged by these tests, treatment NC-12C shows the largest increase. However, these values can also depend on the deposition of the consolidant inside the structure. If the consolidant is well distributed in the sample volume and placed between the grain contacts, it can attain higher values. Nevertheless, those high values may not correspond with the macroscopic mechanical strength, as the cohesion of the consolidant itself might be poor. Therefore, splitting tensile strength tests have been done to confirm mechanical performance. In those tests, it was evident that the consolidant with the highest mechanical strength gain was NC-25C, followed by NC-12C, itself followed closely by NC-29C. The reason for this result lies most probably in the solid content after curing. Notably, the solid content after curing for NC-25C was two to four times higher than those of the other consolidants (see Table 1). If more consolidator solids remain in the stone matrix, it is likely that the strength will increase that much more. Earlier studies of a similar type, in which different alkoxysilanes with varying gel deposition rates were tested, confirm this hypothesis [39]. The amount of consolidant deposited inside the structure is the governing aspect for the mechanical strength gain. Moreover, the same trend can be confirmed through the drilling resistance measurements in Fig. 7. In those measurements, NC-25C showed the highest value, followed by lower drilling resistance values observed for NC-29C and NC-12C.

All three treatments showed an essential gain with respect to mechanical strength in laboratory and on-site measurements. To determine the possibility of harmful over-consolidation effects, additional studies concerning the compatibility of the treatments (e.g. water vapour diffusion tests, durability tests, etc.) need to be done in the laboratory with comparable depth distributions of consolidants.

4. Conclusions

The aim of the present study was to analyse the distribution depth of stone consolidants applied on-site after curing and to mathematically model, with an analytical approach, the concentration of the consolidants' solid content as a function of depth within the stone. Three consolidants were applied on a historical façade of St. Stephen's Cathedral in Vienna, Austria. The drilled cores examined by SEM and image analysis showed that all consolidants exhibited an exponential decline of consolidant solid content with increasing depth into the stone, being highest on the surface and subsurface area and declining towards the inner part of the structure to different extents. The model based on a version of one-dimensional Fick's second law successfully describes the depth distribution, allowing improved interpretations and performance indicators for different stone consolidation treatments. We conclude that capillary forces, acting upon drying, are the governing factor for the distribution of the consolidants within water-based nano-zirconia and water–alcohol-based colloidal silica. For reactive alkoxysilane, capillary forces acting upon drying are less pro-

nounced, which is why such consolidants exhibit a more homogeneous depth distribution. Furthermore, we determine that drilling resistance measurements performed on-site, in the vicinity of the bore holes where the drilled cores have been extracted, confirm the modelled and image-analysed findings. Young's modulus and splitting tensile strength tests on laboratory-treated specimens further confirm the mechanical strength gain assessed through drilling resistance measurements. Finally, we hope that the present study lays a foundation for systematic activities of modelling in the area of stone consolidation, which is lacking in published research and is urgently needed in order to address the complexity of a given treatment's outcome.

CRediT authorship contribution statement

Matea Ban: Conceptualization, Data curation, Formal analysis, Investigation, Methodology, Validation, Visualization, Writing - original draft. **Laura Aliotta:** Conceptualization, Data curation, Formal analysis, Investigation, Methodology, Validation, Writing - review & editing. **Vito Gigante:** Conceptualization, Data curation, Formal analysis, Investigation, Methodology, Validation, Writing - review & editing. **Elisabeth Mascha:** Investigation, Methodology, Writing - review & editing. **Antonella Sola:** Investigation, Methodology, Writing - review & editing. **Andrea Lazzeri:** Conceptualization, Funding acquisition, Project administration, Supervision, Writing - review & editing.

Funding Sources

The authors acknowledge TU Wien University Library for financial support through its Open Access Funding Programme. The consolidants studied in the present work have been developed through the supported by the 'Nano-Cathedral' project, funded by the European program Horizon 2020 Call NMP21-AC "Nanomaterials for conservation of European architectural heritage developed by research on characteristic lithotypes" (GA 646178).

Declaration of Competing Interest

The authors declare that they have no known competing financial interests or personal relationships that could have appeared to influence the work reported in this paper.

Acknowledgements

Cecilia Pesce and Lukas Achleitner are gratefully acknowledged for their support in the lab. We thank Peter Urbanek and Paul Sonnleitner for proofreading and generally supporting this work. Johannes Weber and Andreas Rohatsch are recognised for their help in discussing the data. The authors thank Colorobbia S.p.A (Italy) for the supplied consolidant NC-12C, Technologia Navarra de Nanoproductos, S.L. - Tecnan (Spain) for NC-29C and ChemSpec S.R.L. (Italy) for NC-25C.

Appendix I

Equation (11) is a computed solution, using WolframAlpha LLC (Software Mathematica), while equation (12) is analytically derived. In the following, the mathematical rearrangement from the analytical solution to the computed answer is shown:

$$c(x) = \frac{(C_L - C_0)\cdot e^{-ABx} - (C_L - C_0) + C_0 \cdot (e^{-ABL} - 1)}{e^{-ABL} - 1} \tag{A1}$$

$$c(x) = \frac{C_L \cdot e^{-ABx} - C_0 \cdot e^{-ABx} - C_L + C_0 + C_0 \cdot e^{-ABL} - C_0}{e^{-ABL} - 1} \cdot \frac{-e^{+ABL}}{-e^{+ABL}} \tag{A2}$$

$$c(x) = \frac{-C_L \cdot e^{-ABx} \cdot e^{+ABL} + C_0 \cdot e^{-ABx} \cdot e^{+ABL} + C_L \cdot e^{+ABL} - C_0 \cdot e^{-ABL} \cdot e^{+ABL}}{e^{+ABL} - 1} \tag{A3}$$

$$c(x) = \frac{C_0 \cdot \left(e^{-ABx} \cdot e^{+ABL} - 1\right) + C_L \cdot \left(e^{+ABL} - e^{-ABx} \cdot e^{+ABL}\right)}{e^{+ABL} - 1} \tag{A4}$$

$$c(x) = \frac{C_0 \cdot \left(e^{-ABx} \cdot e^{+ABL} - e^{-ABx} \cdot e^{+ABx}\right) + C_L \cdot \left(e^{+ABL} \cdot e^{-ABx} \cdot e^{+ABx} - e^{-ABx} \cdot e^{+ABL}\right)}{e^{+ABL} - 1} \tag{A5}$$

$$c(x) = \frac{e^{-ABx} \cdot \left[C_0 \cdot \left(e^{+ABL} - e^{+ABx}\right) + C_L \cdot e^{+ABL} \cdot \left(e^{+ABx} - 1\right)\right]}{e^{+ABL} - 1}. \tag{A6}$$

Corresponding constants obtained though Eq. (11) and Eq. (12) as well as the modelled curves can be observed in Table A.1 and Fig. A.1.

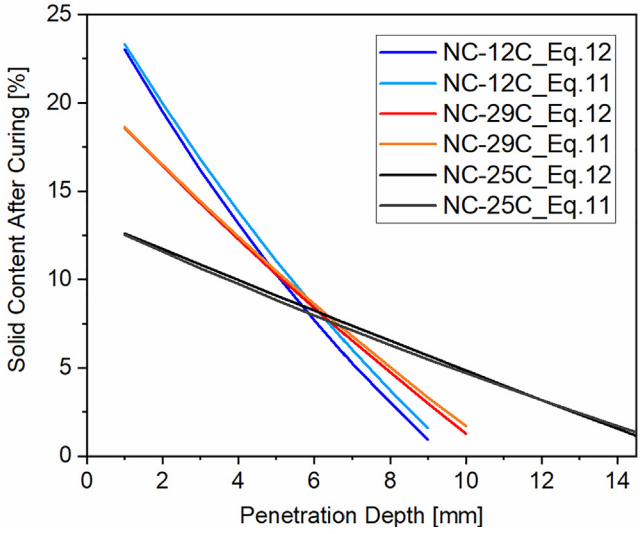

Fig. A1. Comparison between the modelled curves obtained though the computed solution (Eq. (11)) or the analytical model (Eq. (12)) for treatments NC-12C (nano-silica), NC-29C (nano-zirconia) and NC-25C (titania-modified alkoxysilane).

Table A1
Comparison between constants *A*, calculated from image analysis, and *B*, iterated through the computed solution (Eq. (11)) or the analytical model (Eq. (12)), respectively. Constants C_1 to C_3 assess a treatments performance, as evaluated through the modified exponential function using Eq. (13).

Treatment	*A* (Eq.11)	*B* (Eq.11)	*A* (Eq.12)	*B* (Eq.12)	C_1 (Eq.13)	C_2 (Eq.13)	C_3 (Eq.13)
NC-25C (HFES70)	0.09	0.23	0.09	0.08	−28.042	41.555	0.024
NC-12C (ZG12)	0.09	0.63	0.09	0.85	−30.936	57.849	0.064
NC-29C (ZR110)	0.04	0.62	0.04	0.69	−53.270	74.096	0.031

References

[1] J. Brus, P. Kotlik, Consolidation of stone by mixtures of alkoxysilane and acrylic polymer, Stud. Conserv. 41 (2) (1996) 109–119, https://doi.org/10.1179/sic.1996.41.2.109.

[2] R. Ševčík, P. Šašek, A. Viani, Physical and nanomechanical properties of the synthetic anhydrous crystalline CaCO3 polymorphs: vaterite, aragonite and calcite, J. Mater. Sci. 53 (6) (2017) 4022–4033, https://doi.org/10.1007/s10853-017-1884-x.

[3] S.C. De la Rosa-García, A.F. Fuentes, S. Gómez-Cornelio, U. Zagada-Domínguez, P. Quintana, Structural characterization of antifungal CaZn2(OH)6·2H2O nanoparticles obtained via mechanochemical processing, J. Mater. Sci. 53 (19) (2018) 13758–13768, https://doi.org/10.1007/s10853-018-2327-z.

[4] D.S. Facio, J.A. Ordonez, M.L.A. Gil, L.A.M. Carrascosa, M.J. Mosquera, New Consolidant-Hydrophobic Treatment by Combining SiO2 Composite and Fluorinated Alkoxysilane: Application on Decayed Biocalcareous Stone from an 18th Century Cathedral, Coatings 8 (5) (2018), https://doi.org/10.3390/coatings8050170.

[5] A.P. Ferreira Pinto, J. Delgado Rodrigues, Consolidation of carbonate stones: Influence of treatment procedures on the strengthening action of consolidants, J. Cult. Heritage 13 (2) (2012) 154–166.

[6] A. Ferreira Pinto, J. Delgado Rodrigues, Stone consolidation: The role of treatment procedures, J. Cult. Heritage 9 (1) (2008) 38–53, https://doi.org/10.1016/j.culher.2007.06.004.

[7] F. Braun, J. Orlowsky, Effect of Different Silicic Acid Ester on the Properties of Sandstones with Varying Binders, Restorat. Build. Monum. 23 (1) (2018) 1–13, https://doi.org/10.1515/rbm-2017-0003.

[8] G. Borsoi, B. Lubelli, R. van Hees, R. Veiga, A.S. Silva, L. Colla, L. Fedele, P. Tomasin, Effect of solvent on nanolime transport within limestone: How to improve in-depth deposition, Colloids Surf., A 497 (2016) 171–181, https://doi.org/10.1016/j.colsurfa.2016.03.007.

[9] J. Delgado Rodrigues, A. Grossi, Indicators and ratings for the compatibility assessment of conservation actions, J. Cult. Heritage 8 (1) (2007) 32–43, https://doi.org/10.1016/j.culher.2006.04.007.

[10] M. Ban T. De Kock F. Ott G. Barone A. Rohatsch S. Raneri Neutron Radiography Study of Laboratory Ageing and Treatment Applications with Stone Consolidants Nanomaterials (Basel) 9 4 2019 10.3390/nano9040635

[11] G. Graziani, C. Colombo, C. Conti, E. Possenti, E. Perelli Cippo, M. Realini, E. Sassoni, Neutron radiography as a tool for assessing penetration depth and distribution of a phosphate consolidant for limestone, Constr. Build. Mater. 187 (2018) 238–247, https://doi.org/10.1016/j.conbuildmat.2018.07.173.

[12] F. Hameed, B. Schillinger, A. Rohatsch, M. Zawisky, H. Rauch, Investigations of stone consolidants by neutron imaging, Nucl. Instrum. Methods Phys. Res., Sect. A 605 (1–2) (2009) 150–153, https://doi.org/10.1016/j.nima.2009.01.139.

[13] C. Conti, C. Colombo, G. Festa, J. Hovind, E.P. Cippo, E. Possenti, M. Realini, Investigation of ammonium oxalate diffusion in carbonatic substrates by neutron tomography, J. Cult. Heritage 19 (2016) 463–466, https://doi.org/10.1016/j.culher.2015.12.005.

[14] M. Slavíková, F. Krejčí, J. Žemlička, M. Pech, P. Kotlík, J. Jakůbek, X-ray radiography and tomography for monitoring the penetration depth of consolidants in Opuka – the building stone of Prague monuments, J. Cult. Heritage 13 (4) (2012) 357–364, https://doi.org/10.1016/j.culher.2012.01.010.

[15] M. Lanzón, V.E. García-Vera, A.J. Tenza-Abril, V. De Stefano, Use of image analysis to evaluate surface dispersion and covering performance of nanolime coatings sprayed on heritage material substrates, Appl. Surf. Sci. 480 (2019) 962–968, https://doi.org/10.1016/j.apsusc.2019.03.066.

[16] H. Pape, C. Clauser, J. Iffland, Permeability prediction based on fractal pore-space geometry, Geophysics 64 (5) (1999) 1447–1460, https://doi.org/10.1190/1.1444649.

[17] B. Berkowitz, I. Dror, S.K. Hansen, H. Scher, Measurements and models of reactive transport in geological media, Rev. Geophys. 54 (4) (2016) 930–986, https://doi.org/10.1002/2016rg000524.

[18] G.K. Darbha, C. Fischer, J. Luetzenkirchen, T. Schafer, Site-specific retention of colloids at rough rock surfaces, Environ. Sci. Technol. 46 (17) (2012) 9378–9387, https://doi.org/10.1021/es301969m.

[19] 19. Rohatsch A (2005) Neogene Bau-und Dekorgesteine Niederösterreichs und des Burgenlandes. In: Schwaighofer, B., Eppensteiner,W. (Eds.), "Junge" Kalke, Sandsteine und Konglomerate — Neogen. Mitteilungen IAG BOKU, pp. 27-31.,

[20] D. Benedetti, E. Bontempi, R. Pedrazzani, A. Zacco, L.E. Depero, Transformation in calcium carbonate stones: some examples, Phase Transitions 81 (2–3) (2008) 155–178, https://doi.org/10.1080/01411590701514342.

[21] 21. Ban M, Baragona A, Ghaffari E, Weber J, Rohatsch A (2016) Artificial aging techniques on various lithotypes for testing of stone consolidants. Paper presented at the Science and Art: A Future for Stone: Proceedings of the 13th International Congress on the Deterioration and Conservation of Stone, Volume 1. Paisley: University of the West of Scotland; Hughes, J., & Howind, T. (Eds.); 2016,

[22] E. Franzoni, E. Sassoni, G.W. Scherer, S. Naidu, Artificial weathering of stone by heating, J. Cult. Heritage 14 (3) (2013) E85–E93, https://doi.org/10.1016/j.culher.2012.11.026.

[23] J. Lukaszewics, D. Kwiatkowski,M. Klingspor, Consolidation of Gotland stone in monuments Methods of evaluating products for the conservation of porous building materials in monuments: preprints of the international colloquium, Rome, 19–21, 1995, 1995, 179-187.

[24] L. Normand, S. Duchêne, V. Vergès-Belmin, C. Dandrel, D. Giovannacci, W. Nowik, Comparative in Situ Study of Nanolime, Ethyl Silicate and Acrylic Resin for Consolidation of Wall Paintings with High Water and Salt Contents at the Chapter Hall of Chartres Cathedral, Int. J. Architect. Heritage 1–14 (2020), https://doi.org/10.1080/15583058.2020.1731628.

[25] F. Papadopulos, M. Spinelli, S. Valente, L. Foroni, C. Orrico, F. Alviano, G. Pasquinelli, Common tasks in microscopic and ultrastructural image analysis using ImageJ, Ultrastruct. Pathol. 31 (6) (2007) 401–407, https://doi.org/10.1080/01913120701719189.

[26] 26. CEN (2004) Standard EN 14146, Determination of dynamic elastic modulus by measuring the fundamental resonant frequency.

[27] 27. ASTM International WC, USA (2008) ASTM D 3967–08, Standard test method for splitting tensile strength of intact rock core specimens.

[28] Y.M. Volfkovich, A.N. Filippov, V.S. Bagotsky, Structural properties of porous materials and powders used in different fields of science and technology, Springer (2014), https://doi.org/10.1007/978-1-4471-6377-0.

[29] A. Filippov, V. Starov, D. Llyod, S. Chakravarti, S. Glaser, Sieve mechanism of microfiltration, J. Membr. Sci. 89 (3) (1994) 199–213, https://doi.org/10.1016/0376-7388(94)80102-9.

[30] A.N. Filippov, R.K. Iksanov, Mathematical modeling of microfiltration of polydisperse suspension on heterogeneous membranes, Pet. Chem. 52 (7) (2012) 520–526, https://doi.org/10.1134/s0965544112070043.

[31] J. Happel, H. Brenner, Low Reynolds number hydrodynamics: with special applications to particulate media, Springer Science & Business Media, 2012.

[32] Barenblatt GI, Entov VM, Ryzhik VM (1989) Theory of fluid flows through natural rocks.

[33] J. Šperl, J. Trčková, Permeability and porosity of rocks and their relationship based on laboratory testing, Acta Geodyn. Geomater. 5 (149) (2008) 41–47.

[34] Brace W Permeability of crystalline and argillaceous rocks. In: International Journal of Rock Mechanics and Mining Sciences & Geomechanics Abstracts, 1980. vol 5. Elsevier, pp 241-251. doi:10.1016/0148-9062(80)90807-4

[35] C. Franzen, P.W. Mirwald, Moisture content of natural stone: static and dynamic equilibrium with atmospheric humidity, Environ. Geol. 46 (3–4) (2004), https://doi.org/10.1007/s00254-004-1040-1.

[36] M. Drdacky, J. Lesak, S. Rescic, Z. Slizkova, P. Tiano, J. Valach, Standardization of peeling tests for assessing the cohesion and consolidation characteristics of historic stone surfaces, Mater. Struct. 45 (4) (2012) 505–520, https://doi.org/10.1617/s11527-011-9778-x.

[37] M. Remzova, R. Zouzelka, J. Lukes, J. Rathousky, Potential of Advanced Consolidants for the Application on Sandstone, Applied Sciences 9 (23) (2019), https://doi.org/10.3390/app9235252.

[38] M. Drdácký, Testing Efficiency of Stone Conservation Treatments. In: Majid H, Ioannis K (eds) Advanced Materials for the Conservation of Stone. Springer, 2018. pp 175-184, ISBN 978-173-319-72259-72257.

[39] M. Ban, E. Mascha, J. Weber, A. Rohatsch, J.D. Rodrigues, Efficiency and Compatibility of Selected Alkoxysilanes on Porous Carbonate and Silicate Stones, Materials (Basel) 12 (1) (2019), https://doi.org/10.3390/ma12010156.